

# Diagnosis of power losses in PV plants by means of UAV thermography

A.P. Catalano, V. d'Alessandro, P. Guerriero, S. Daliento

Department of Electrical Engineering and Information Technology, University of Naples "Federico II" Via Claudio 21, 80125 Napoli, Italy; Phone: +39-081-7683122; e-mail: pierluigi.guerriero@unina.it

**Abstract**— This paper presents a technique to relate the temperature distribution over solar panel, achievable by means of the UAV thermography, with the electrical power distribution which is the cause of those temperatures. Differently from a mere thermal analysis, that can only identify "hotter" regions throughout the solar field, this technique allows evaluating electrical power losses associated to malfunctioning events. The method is based on the energy balance between the sun irradiance, which tends to heat up the solar cells, and the electrical behavior, which tends to cool down if the cell is converting light, while tends to further increase the cell temperature in those cases in which the cell behaves as a load. The reliability of the technique is evidenced by providing simulated thermal maps, achieved by means of known electrical and irradiance conditions, which are analyzed to re-achieve the starting electrical condition at the single cell level.

**Index Terms**—Hot spot, partial shading, thermal analysis, photovoltaics, UAV.

## I. INTRODUCTION

It is well known that outlier solar cells can dramatically reduce the functionality and the energy revenues achievable by photovoltaic (PV) plants [1-4]. Since many kinds of possible faults induce the rising in temperature of the solar panel (often of only a part of it), thermal analysis is one of the most widely employed technique for the localization of malfunctioning solar panels and cells in wide solar fields [5-6]. Some of those faults can be easily detected because the overheating is extremely significant and very concentrated in space (hot-spot); some others, produce a diffuse rising in temperature but much less significant. Unfortunately, analogous behaviors can be caused by "normal" events, like architectural shadowing or localized accumulation of grime. To distinguish between real faults and normal events is not an easy task, as proved by the numerous diagnosis approaches that have been proposed so far in the recent literature [7-11]. Such approaches can be roughly classified in terms of allowed granularity: high-granularity are those methods that try to inspect, up to the single cell, the operation of a solar system; usually, such techniques require the presence of devised sensors equipping PV panes so that they have the main disadvantage to be very costly. On the other side, almost all PV systems are provided with some form of low granularity monitoring feature, consisting in the capability to collect the delivered power and current of sections of the PV field up to the entire plant. The second approach is, obviously, totally insensitive to local faults.

From this point of view, thermal maps, that have the advantage to be achievable by means of unmanned aerial vehicles (drones), combine the capability to "see" the thermal behavior of PV systems at the sub-cell level, with the availability of a global view of the whole plant.

As said before, fault localization by means of thermal maps is based on the widely accepted opinion for which heating is deeply related to the malfunctioning.

However, it has never been tried to relate the amount of over-temperature to the electrical power which is being dissipated. In other terms, even though uneven heating is always caused by uneven electrical behavior, the link between thermal maps and the electrical operation has never been investigated. Such information could be of paramount importance because could allow the quantification of the electrical issue associated to the thermal evidence. The evaluation of the electrical power dissipation could also be exploited to quantify, in terms of economic revenues, to assess the convenience of the fault fixing intervention, thus skipping those faults causing negligible losses.

In this paper the power balance equation is exploited to estimate the electrical power either dissipated or generated by each solar cell belonging to a solar panel whose thermal map has been captured by an aerial vehicle. As a consequence, it is possible to link the thermal behavior to the electrical operation, thus allowing reliable diagnostic about the healthy status of the solar panel. The reliability of the method is evidenced by means of accurate three-dimensional numerical simulations taking advantage of the COMSOL environment, in which, in order to achieve extremely realistic operation, detailed models describing the actual structure of a solar panel have been implemented. The temperature distribution evaluated by COMSOL under various operating conditions have been treated as experimental thermal maps that have been elaborated by means of the power balance approach. Differently from real experiments, this approach has the advantage that the results that should be achieved are known (because corresponding to the operating conditions that have been set), thus allowing the reliable estimation of the discrepancy between the results of the model compared to the exact expected results.

The paper is organized as follows. In Section II details about the COMSOL description of the assigned structure, are given. Section III gives details of the analytical model developed to evaluate the electrical power at the cell level

starting from temperature information. Section IV describes simulated experiments. Conclusions are drawn in Section V.

## II. SIMULATION STRUCTURE

For simulation purposes a solar panel characterized by previously assessed mechanical structure and thermal properties of all component materials, has been chosen. A photograph is shown in Fig.1



Fig. 1. Solar panel under study.

This solar panel embeds 40 series-connected solar cells of the mono-crystalline type. The series is in turn made of two groups formed by 20 solar cells. Each group is protected by a bypass diode hosted in the junction box located in the rear side of the solar panel [12-14].

As can be argued from the figure each solar cell is made by half silicon wafer (thus reducing the current and increasing the voltage available in the occupied space). The width of the solar panel is 55.5 cm while the height, is 71.9 cm, above measures includes the aluminum frame, whose thickness is 3.4 cm.

As usual solar cells are sandwiched between a layer of EVA (ethylene vinyl acetate), whose thickness is 0.95 mm, and the Tedlar back sheet, whose thickness is 1 mm. Above the EVA layer, whose main role is to soften the impact of mechanical stress, the cells are covered by a high optical transmittance glass plate, having a thickness of 3 mm. The area of each solar cell is 72.8 cm<sup>2</sup>.

The structure of the solar panel with numbered cells is sketched in Fig. 2.

Such a numbering will be exploited in the following of the paper to clearly individuate the solar cells and their operating conditions.

As said in the previous section the real structure of the solar panel was discretized in the COMSOL environment, which solves the thermal problem on the basis of the finite-element method. In particular, nonlinear 3-D thermal simulations were performed on the mesh structure reported in Fig. 3.

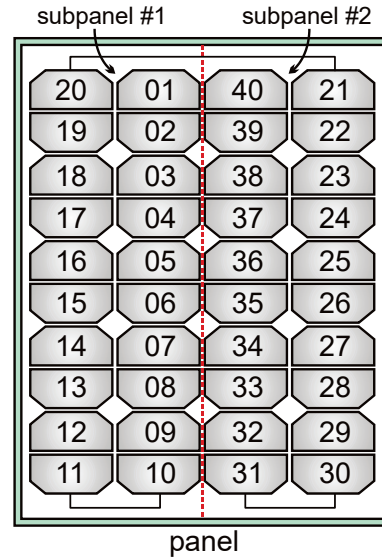


Fig. 2. Solar panel schematization and cell numbering

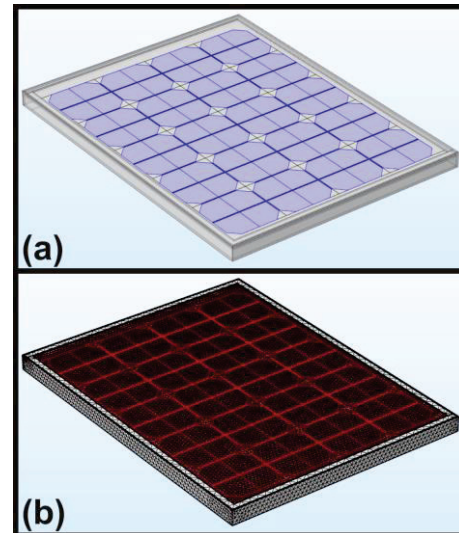


Fig. 3. Solar panel (a) and corresponding COMSOL mesh (b).

For illustrative purposes the image does not show the tempered glass and EVA layer, which were actually taken into account in the simulations.

In order to reproduce, by means of simulations, reliable data (similar to those that would be achieved in real experiments), the electrical performance of the real solar panel was considered. Under standard test conditions (solar irradiance of 1000 W/m<sup>2</sup>, 1.5 Air Mass, and cell temperature of 25°C), the solar panel supplied an open circuit voltage of 24.6 V and a corresponding maximum power point (MPP) voltage of 20.2 V. The short circuit current was 2.81 A and the corresponding current at the MPP was 2.48 A. These characteristics were exploited to adjust a proper circuit model of the solar panel in which each solar cell is described by means of the one diode equivalent circuit. The adjusted model allowed the evaluation of the electrical power, either produced or dissipated by each solar cell under various

irradiance conditions. Since the solar panel was described at the single cell level, uneven irradiance conditions were allowed, so that, as an example, partial shading conditions (bringing to the hot-spot formation) were correctly emulated. Circuit simulations were performed in the PSpice environment; the electrical power provided by these simulations were summed to the solar irradiance impinging on each solar cell. The total power associated to each solar cell was converted in the COMSOL structure in a corresponding number of heat sources, geometrically coinciding with the solar cells. The output of the COMSOL simulations were thermal maps definitively analogous to those achievable by means of infrared thermography. The purpose of the analysis reported in the following section is to obtain the electrical power distribution that generated the given map.

### III. ANALYTICAL APPROACH

The approach for the identification of the electrical powers of the individual cells, starting from the knowledge of the temperature distribution on the front side of the solar panel, relies on the idea that the temperature increment (or decrement) of each solar cell is given by the balance of the impinging power irradiance, the electrical power produced inside the solar cell and the thermal power exiting from the solar cell.

The above idea can be represented by means of the following balance equation applied to the  $i$ -th cell:

$$\Delta T_i = k_i (G_i \cdot A_{cell} - P_i - P_{out,i}) \quad (1)$$

in this equation  $G_i$  is the irradiance actually reaching the solar cell area  $A_{cell}$  (i.e. taking into account the reflection from the glass surface),  $P_i = V_i \cdot I_i$  is the electrical power generated (or absorbed) by the solar cell; it is subtracted from the irradiance because it corresponds to the share of sun energy converted into electrical power (conversely, if this term is negative means that the solar cell is behaving as a load, thus increasing the cell temperature).  $P_{out,i}$  is the thermal power flowing toward the neighboring cells. The terms  $k_i$  take into account heat dispersion through the glass in the vertical direction; they are fitting parameters which are determined by means of the calibration procedure described in the following section. The model takes into account the fact that every solar cell is mutually coupled with all other solar cell; in other terms, every solar cell contributes to the heating of the others and is heated by the others.  $\Delta T_i$  is defined as  $T_i - T_{amb}$ ,  $T_i$  being the cell temperature and  $T_{amb}$  the ambient temperature.

In the above equation the evaluation of the term  $P_{out,i}$  is the critical issue. To this end, the lateral heat propagation has been assumed to entirely occur through the glass plate (this assumption is realistic because solar cells are laterally spaced inside the solar panel); as a consequence  $P_{out,i}$  can be evaluated from the gradient of the front temperature distribution according to

$$P_{out,i} = k_{glass} \cdot t_{glass} \cdot \oint_{E_i} \nabla T_{front} \cdot \hat{n} dl \quad (2)$$

where  $E_i$  is the lateral boundary of the cell,  $\hat{n}$  is the outward-pointing unit normal vector, and  $t_{glass}$  is the thickness of the glass.

Since the front temperature field  $T_{front}$ , is assumed to be known, because determined by aerial thermal images, equations (1) and (2) allows determining the distribution of the electrical power  $P_i$  generated or dissipated by each solar cell. In particular, the electrical power dissipated as a consequence of a malfunctioning event can be determined on the basis of the mere knowledge of the temperature map.

### IV. SIMULATED EXPERIMENTS

The temperature reached by the surface of a solar cell depends both on operating conditions and on crystalline defects that can be present either the bulk semiconductor and on surfaces [15-19]. The method illustrated in the previous section has been applied to two case studies. The first one refers to the presence, in the solar panel, of a single damaged solar cell; the second case is the classical hot spot generated by the partial shadowing of a solar cell. approach was applied to identify the  $P_i$  distribution in a panel with a single damaged cell.

The damage in the solar cell was emulated by setting a low value for the shunt resistance [20] in the equivalent circuit corresponding to the solar cell. As explained in Section II, the first step of the procedure has been the evaluation, by means of PSpice, of the electrical power generated or absorbed by each solar cell, this power contributed to the heat generation in the COMSOL environment.

The output of the COMSOL simulation for this case is shown in Fig.4 in the form of a thermal map.

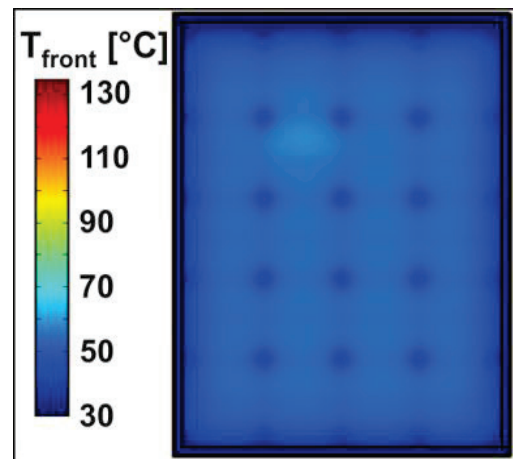


Fig. 4. Thermal map evaluated by COMSOL when cell #3 has a low shunt resistance.

As can be seen, solar cell #03 (the one with the reduced shunt resistance) shows a slight increment of the temperature. As can be inferred from Fig.5, that reports the average temperatures over the solar cells, this

increment is about three degrees above the average temperature of other cells. In order to pass, from the temperature map, to the electrical power that originated such a map, it is important to note that in (1) the terms  $k_i$ , depending on the particular solar cell, are not known. This means that a preliminary calibration is needed to determine these values. The calibration can be performed by assuming the availability of the thermal map of a solar panel operating under normal conditions (no damaged cells, no shadows) at the MPP. In such a case the power is evenly shared among the cells. From the distribution of the front temperatures the average temperatures  $T_i$  appearing in (1) can be determined; at the same time the gradient  $\nabla T_{front}$  can be determined as well. From the gradient (2) allows the evaluation of  $P_{out,i}$ , so that, by returning in (1),  $k_i$  can be evaluated.

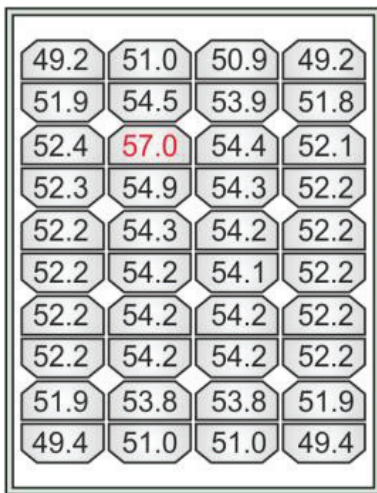


Fig. 5. Average front temperatures corresponding to the thermal map of Fig.4

Once  $k_i$  have been achieved (1) and (2) can be exploited to compute the terms  $P_i$  corresponding to each solar cell. The result is shown in Fig. 6.

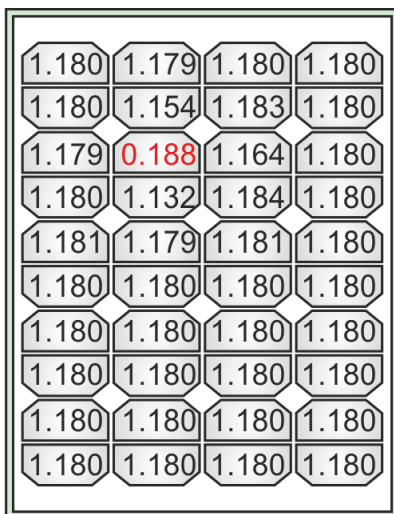


Fig. 6. Electric powers [W] evaluated by (1) on the base of the thermal map of Fig.4.

As can be seen, the temperature increment of cell #3 is dictated by the decreasing, with respect to the normal operating solar cells, of the converted electrical power. It is interesting to note that it is correctly revealed that, actually, the cell does not dissipate power, it just works with a lower efficiency.

The second experiment was conducted by assuming that a solar cell was subject to a shadow covering 20% of its area. In this case the subpanel is pushed to bypass; under this condition, as confirmed by the electrical simulations, all the cells belonging to the bypassed subpanel operate close to the MPP, whereas cell #3 behaves like a load.

The temperature map evaluated by COMSOL for this case is shown in Fig. 7. As expected, a dramatic increase in the temperature of cell #3 is found in this case, with an hot spot temperature above 120°C and an average temperature over the cell of about 110°C. It is interesting to note that the model implemented in COMSOL correctly describe the heating up of the neighboring cells, which are subject to the thermal coupling with the shaded cell.

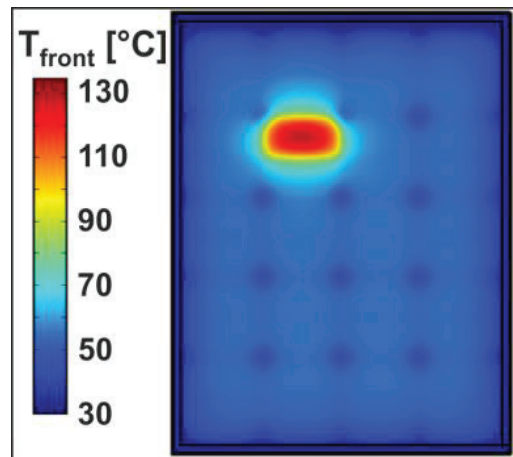


Fig. 7. Thermal map evaluated by COMSOL when cell #3 is partially shaded.

The electrical power distribution evaluated for this case is shown in Fig. 8. As can be seen, the term  $P_i$  corresponding to the shaded cell is negative and quite high; in fact, it is correctly evaluated as nearly equal to the sum of the power delivered by the sunny cells. It is also interesting to note that, even though the neighboring cells are hot, they do not dissipate power; indeed, their temperature depend on the proximity with the shaded cell, the power they deliver is lower because of the inverse dependence on temperature.

The analysis of the electrical power map leads to the conclusion that the subpanel is bypassed, so that it can be evaluated how the shadow affects the energy produced by the solar field.

1.147	1.127	1.180	1.171
1.154	0.780	1.236	1.179
1.173	-19.3	0.915	1.181
1.157	0.411	1.254	1.181
1.157	1.132	1.191	1.181
1.149	1.146	1.180	1.180
1.150	1.151	1.180	1.180
1.150	1.151	1.180	1.180
1.150	1.151	1.180	1.180
1.150	1.150	1.180	1.181

Fig. 8. Electric powers [W] evaluated by (1) on the base of the thermal map of Fig.7.

## V. CONCLUSIONS

In this paper a technique suited to evaluate the electrical power delivered or dissipated by single solar cells embedded in series connected solar panel has been presented. The method relies on the availability of thermal maps achieved by means of UAV thermography and relates temperature information with local electrical power. Simulated experiments have shown the capability of the method to individuate both damaged solar cells, not causing significant power losses, and limiting solar cells, leading the solar panel into bypass.

## REFERENCES

- [1] Review of Failures of Photovoltaic Modules ISBN 978-3-906042-16-9 Report IEA-PVPS T13-01:2014
- [2] D. DeGraaff, R. Lacerda, Z. Campeau, "Degradation Mechanisms in Si Module Technologies Observed in the Field; Their Analysis and Statistics" NREL 2011 Photovoltaic Module Reliability Workshop Golden, Colorado
- [3] E. Kaplani, "Degradation effects in sc-Si PV modules subjected to natural and induced ageing after several years of field operation," *Journal of Engineering Science and Technology Review*, vol. 5, no. 4, pp. 18–23, 2012
- [4] A Livera, M. Theristis, G. Makrides, and G. E. Georghiou, "Recent advances in failure diagnosis techniques based on performance data analysis for grid-connected photovoltaic systems," *Renewable Energy*, vol. 133, pp. 126–143, 2019
- [5] M. Simon and E. L. Meyer, "Detection and analysis of hot-spot formation in solar cells," *Solar Energy Materials & Solar Cells*, vol. 94, no. 2, pp. 106–113, 2010
- [6] P. Bellezza Quater, F. Grimaccia, S. Leva, M. Mussetta, and M. Aghaei, "Light Unmanned Aerial Vehicles (UAVs) for cooperative inspection of PV plants," *IEEE Journal of Photovoltaics*, vol. 4, no. 4, pp. 1107–1113, 2014
- [7] F.J. Sánchez-Pacheco, P. J. Sotorrío-Ruiz, J. R. Heredia-Larrubia, F. Pérez-Hidalgo, and M. Sidrach De Cardona, "PLC-based PV plants smart monitoring system: Field measurements and uncertainty estimation," *IEEE Transactions on Instrumentation and Measurement*, vol. 63, no. 9, pp. 2215–2222, 2014
- [8] P. Guerriero, F. Di Napoli, G. Vallone, V. d'Alessandro, and S. Daliento, "Monitoring and diagnostics of PV plants by a wireless self-powered sensor for individual panels," *IEEE Journal of Photovoltaics*, vol. 6, no. 1, pp. 286–294, 2016
- [9] S. Vergura, G. Acciani, V. Amoroso, G. E. Patrono, and F. Vacca, "Descriptive and inferential statistics for supervising and monitoring the operation of PV plants," *IEEE Transactions on Industrial Electronics*, vol. 56, no. 11, pp. 4456–4464, 2009
- [10] P. Guerriero, L. Piegari, R. Rizzo, and S. Daliento, "Mismatch based diagnosis of PV fields relying on monitored string currents," *International Journal of Photoenergy*, vol. 2017, no. 2, 2017
- [11] V. d'Alessandro, F. Di Napoli, P. Guerriero, and S. Daliento, "An automated high-granularity tool for a fast evaluation of the yield of PV plants accounting for shading effects". *Renewable Energy*, **83**, pp. 294-304, (2015).
- [12] E. S. Hasym, S. R. Wenham, M. A. Green, "Shadow tolerance of modules incorporating integral bypass diode solar cells" *Solar Cells*, 19 (1986 - 1987) 109 - 122 109
- [13] D. Chen "Study of crystalline silicon solar cells with integrated bypass diodes" China Technological Sciences, March 2012
- [14] S. Daliento, L. Mele, P. Spirito, R. Carta, and L. Merlin, "Experimental study on power consumption in lifetime engineered power diodes", *IEEE Tran. on Electron Devices*, **56**, no. 11, pp. 2819-2824, (2009).
- [15] S. Daliento, L. Mele, E. Bobeico, L. Lancellotti, P. Morvillo, "Analytical modelling and minority current measurements for the determination of the emitter surface recombination velocity in silicon solar cells", *Solar Energy Material and Solar Cells* 91 (8), pp. 707-713, 2007.
- [16] S. Daliento, L. Mele, "Approximate closed-form analytical solution for minority carrier transport in opaque heavily doped regions under illuminated conditions", *IEEE Transaction on Electron Devices*, Vol. 53, no. 11, pp. 2837-2838, 2006.
- [17] S. Bellone, G.D. Licciardo, S. Daliento, L. Mele, "Experimental measurements of majority and minority carrier lifetime profile in SI epilayers by the use of an improved OCVD method", *IEEE Electron Devices Letters*, Vol. 26, no 7, pp. 501-503, 2005.
- [18] A. Cutolo, S. Daliento, A. Sanseverino, G. Vitale, L. Zeni, "An optical technique to measure the bulk lifetime and the surface recombination velocity in silicon samples based on a laser diode probe system" *Solid State Electronics*, Volume 42, 6, pp 1035-1038 June 1998.
- [19] S. Daliento, A. Sanseverino, P. Spirito, "An improved model for extraction of strongly spatial dependent lifetimes with the ac lifetime profiling technique", *IEEE Transaction on Electron Devices*, Vol. 46, no. 8, pp. 1808-1810, 1999
- [20] V. d'Alessandro, P. Guerriero, S. Daliento, M. Gargiulo, "Accurately extracting the shunt resistance of photovoltaic cells in installed module strings", 3d International Conference on Clean Electrical Power, ICCEP 2011, pp. 164-168, 2011.